INTERNATIONAL JOURNAL OF HYDROGEN ENERGY 44 (2019) 12783–12792

Available online at www.sciencedirect.com

ScienceDirect

journal homepage: www.elsevier.com/locate/he

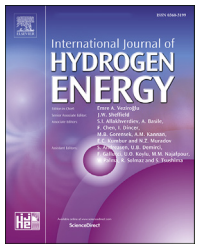

Interleaved, switched-inductor, multi-phase, multi-device DC/DC boost converter for non-isolated and high conversion ratio fuel cell applications

A. Garrigós[*], *D. Marroquí*, *A. García*, *J.M. Blanes*, *R. Gutiérrez*

Industrial Electronics Group, Miguel Hernandez University of Elche, 03202 Elche, Alicante, Spain

ARTICLE INFO

Article history:
Received 12 July 2018
Received in revised form
12 October 2018
Accepted 9 November 2018
Available online 4 December 2018

Keywords:
Interleaved
Switched-inductor
Multi-phase
Multi-device
DC/DC
Fuel cell

ABSTRACT

Fuel cell power conditioners often require high step-up voltage gains to accommodate low input fuel cell voltages into high voltage busses. Traditional non-isolated DC-DC boost converters are unable to offer such as gains because of several parasitic elements and non-ideal behaviour of power semiconductors and driving circuits. Moreover, paralleled converters are also desirable to simplify power-up scaling and to reduce input/output current ripples. In this context, a very versatile non-isolated, high step-up voltage gain, interleaved boost converter is presented in this work. Steady-state analysis, simulation and evaluation of different converter structures are discussed in detail. Finally, a 500-W experimental prototype for Nexa Ballard 1.2 kW fuel cell specifications has been implemented and tested to verify the performance.

Introduction

Low-Voltage Direct-Current (LVDC) is becoming an attractive method of providing electrical power and a way of making possible the access to electricity in many developing countries [1,2]. In contrast to centralized Alternating-Current (AC) systems, where electrical power is generated in large plants and then distributed through high voltage networks and finally converted to lower voltages to final users, LVDC is created nearby to the end consumer. Modern DC electrical loads - e.g. computers, LED lighting, mobile phones and others – suggest the use of DC distribution systems, and on top of that, many renewable power sources are DC by nature, e.g. photovoltaic generators or fuel cells [3]. Avoiding DC-AC-DC conversion improves the overall efficiency and cost.

In this context, DC-DC converters play a key role in renewable LVDC networks, adapting different DC voltage levels, protecting the distribution network and isolating electrical faults, with different requirements for each input source, such as photovoltaic, fuel cells, batteries and supercapacitors. In the case of fuel cells, the most critical issues for the power conditioning electronics are large step-up voltage

* *Corresponding author*. Industrial Electronics Group – IEg, Dpt. Materials Science, Optics and Electronic Technology, Miguel Hernandez University of Elche, Torrevaillo building, Av. Universidad s/n, 03202 Elche, Spain.
E-mail address: augarsir@umh.es (A. Garrigós).

https://doi.org/10.1016/j.ijhydene.2018.11.094
0360-3199/

conversion ratio [4], low fuel cell current ripple [5], high efficiency and reduced cost [6]. At a second level, modularity, scalability, redundancy and reliability are common requests associated to these converters [7].

To meet the needs of moderate step-up voltage conversion ratio, Interleaved Boost Converters (IBCs) are commonly adopted, because of simplicity, input current ripple cancellation, modularity, power sharing and enhanced dynamic response [8]. A further step, and with the aim of improving power density and redundancy in medium and high power converters, typically in the range between several hundred of watts and several hundred of kilowatts, a multi-switch, interleaved boost converter (MIBC) has been also proposed [9]. Unfortunately, these solutions does not really fit with high step-up voltage conversion requirements which require extremely high duty ratio, i.e. voltage gain ratio above three. Different solutions are reported in the literature to overcome this limitation [10,11].

An interleaved two-phase boost with a two-inductor (2-L) switched-inductor network has been already proposed in Ref. [12], but in the present work a generalization of a k-L switched-inductor network is presented with n phases and m power transistors per phase, providing a wider view of the modular, high step-up voltage gain boost converters.

Multi-interleaved, switched-inductor boost converter

The general structure of the proposed multi-interleaved, switched-inductor boost converter (MISIBC) is represented in Fig. 1. This topology exhibits several degrees of freedom to optimize the power electronics conditioner. First, power semiconductor switching frequency and inductor frequency could be decoupled by the number of switches per phase, m, using a multiplexed driving pattern [13]. This fact could be used in several ways, such as, magnetic core optimization, input current ripple reduction, power semiconductor losses distribution and switch reconfiguration [14]. In addition, number of phases, n, operated in interleaving mode also allows power sharing, input current ripple cancellation and power switch optimization. However, typical boost structures are limited in voltage step-up gain. Ideal single inductor boost DC transfer function is Vo/Vin = 1/(1-D), where D is the duty cycle, D = ton/T. Although, high step-up (Vo/Vin) voltage ratio is ideally possible, forcing high duty cycle, this is not feasible from the practical point of view. Parasitic inductor resistance, diode forward voltage drop, limited resolution of the driving signal, gate circuits or control issues finally limit the practical duty cycles, which are in the order of D = 0.5–0.7.

On this basis, and especially for low voltage sources, as fuel cells, high step-up voltage gain converters are very attractive. The proposed switched inductor structure, which has the ability to increase the DC voltage ratio, combined with the other advantages derived from multi-device and interleaving is an interesting option for medium and high power fuel cell power systems.

The generalized switched-inductor network consists on k inductors and 3·(k-1) diodes that connects all the inductors in parallel during the ON-state and connects the inductor in series during the OFF-state.

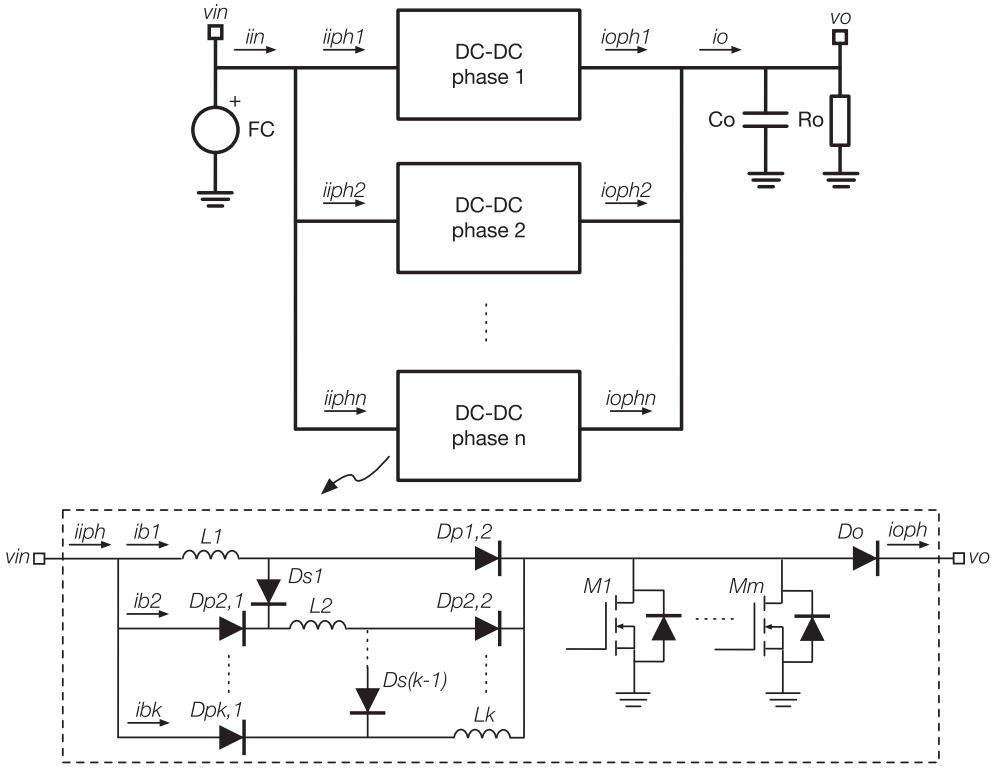

Fig. 1 – Proposed MISIBC DC-DC converter.

MISIBC DC converter analysis

The converter is operated with Pulse Width Modulation (PWM) control and the study is done for Continuous Conduction Mode (CCM) including the forward voltage drop of the diodes (Vd) [15]. The operating principle and the steady-state analysis of CCM is presented in detail as follows.

For each converter phase, two states are identified, ON-state and OFF-state, please refer to Fig. 2. During the ON-state, that is during ton, one of the MOSFETs is turned on. The equivalent circuit, represented in Fig. 2, includes k inductors in parallel with one diode (Vd) in series for the first and the last inductor branches and two diodes (2·Vd) in series for the rest of the inductor branches. Inductors are then charged from the input voltage minus Vd for the first and last branch or 2·Vd in the other inductor branches (1). The output capacitor provides the energy to the load and maintains the output voltage.

$$\begin{aligned} V_L|_{ON-state} &= V_{in} - V_d \quad ;first\ \ and\ \ last\ \ inductor\ \ branch \\ V_L|_{ON-state} &= V_{in} - 2V_d \quad ;others\ \ inductor\ \ branches \end{aligned} \tag{1}$$

During the OFF-state, the output diode provides a free-wheeling current path and all inductors discharge in series to provide energy to the load and recharge the output capacitor. In this mode, k-1 diodes of the switching-inductor network are forward biased and the voltage across a single inductor, assuming equal inductance value for all, is given by (2).

$$V_L|_{OFF-state} = (V_{in} - V_o)/k - V_d \tag{2}$$

Assuming that all inductors exhibit the same inductance value, L, and considering a mid-inductor branch, the volt-second balance on the inductor is expressed as (3).

$$\int_0^{ton} (V_{in} - 2V_d)dt + \int_{ton}^{T/m} \left(\frac{V_{in} - V_o}{k} - V_d\right)dt = 0 \tag{3}$$

By operating (3), the DC voltage gain in CCM is finally given by (4).

$$V_o = V_{in}\left(\frac{1 + (k-1)Dm}{1 - Dm}\right) - kV_d\left(\frac{1 + Dm}{1 - Dm}\right) \tag{4}$$

The DC voltage transfer function of the proposed converter, exhibits larger voltage step-up ratios as the number of inductors, k, increases. A graphical representation of the ideal (Vd neglected) DC voltage gain for k = 1...4 and m = 1 is represented in Fig. 3.

In order to analyse the MISIBC waveforms and component stresses, a representation of a single switched-inductor structure is shown in Fig. 4, where ib_i denotes individual branch current, being i from 1 to k. $Dp_{i,j}$ states for the parallel-inductor connection diodes, being i the number of the branch and j the position within the branch. As observed, $Dp_{1,1}$ and $Dp_{k,2}$ could be avoided to reduce power losses. Ds_i refers to series-inductor connection diodes and input phase current, i_{iph}, is the sum of all branch currents. All the component stresses have been analysed neglecting the diode forward voltage (Vd).

The voltage stress on the parallel-inductor connection power diodes of the switched-inductor network are given by (5) and (6), while the voltage stress on the series-inductor connection diodes of the switched-inductor network is obtained by (7), from $i = 1$ to k.

$$V_{Dpi,1} = \frac{i-1}{k}(V_o - V_{in}) \tag{5}$$

$$V_{Dpi,2} = \frac{k-i}{k}(V_o - V_{in}) \tag{6}$$

$$V_{Dsi} = V_{in} \tag{7}$$

On the other hand, the voltage stress on power MOSFETs and output diode is the same and given by (8).

$$V_M = V_{Do} = V_o \tag{8}$$

From the analysis of the input currents of the switched-inductor network, the average current of the parallel-connection diodes can be expressed in terms of the average inductor current as (9). As the input phase current, i_{iph}, is the sum of all branch currents, the average inductor current is finally represented as a function of the average input current (10). Besides, assuming ideal conversion efficiency and power sharing between phases, average inductor current could be

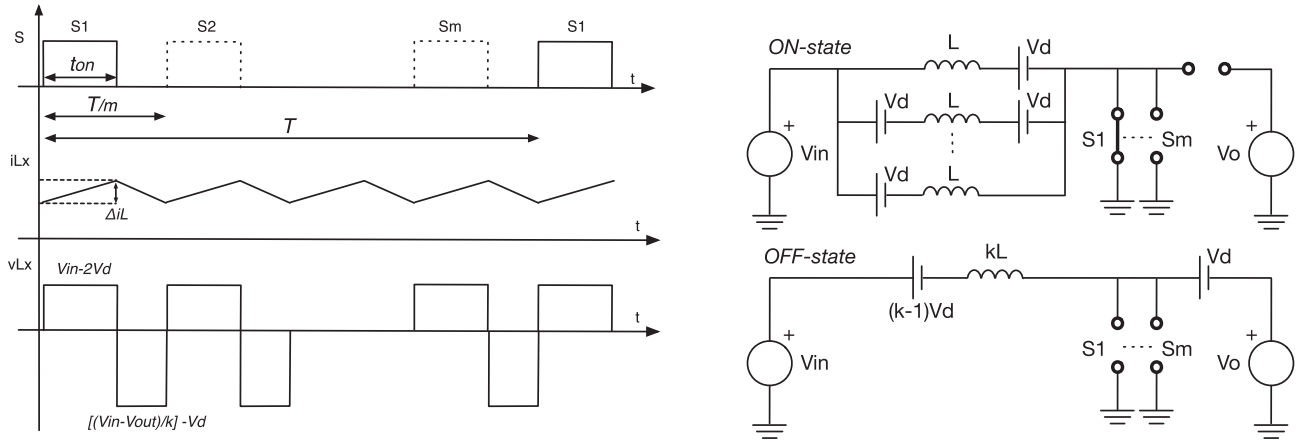

Fig. 2 – Inductor waveforms in CCM operation (left side) and equivalent circuits for ON and OFF states (right side).

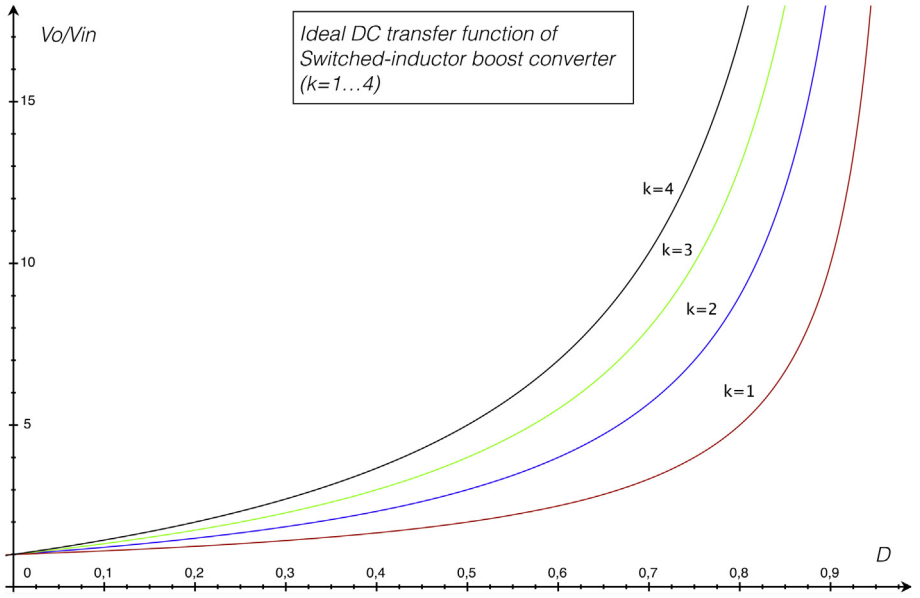

Fig. 3 – DC voltage gain for different k (k = 1...4) and m = 1.

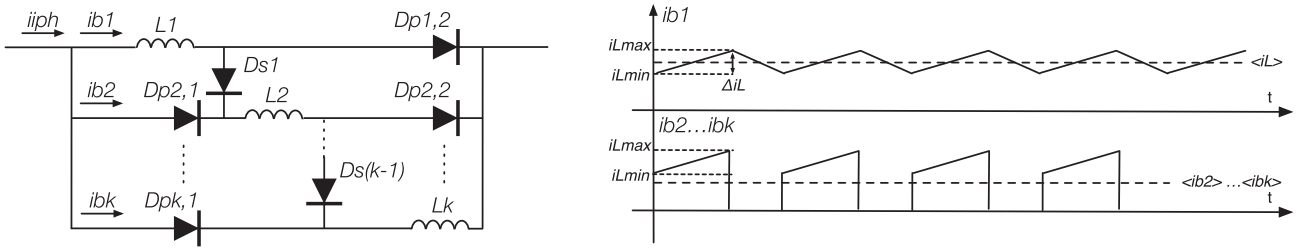

Fig. 4 – Generalized switched-inductor network and input current waveforms.

also expressed in terms of the average output current (11), where *n* represents the number of phases.

$$\begin{array}{c} <i_{b1}> = <i_L> \\ <i_{b2}> .. <i_{bk}> = <i_{Dp}> = Dm<i_L> \end{array} \quad (9)$$

$$<i_L> = \frac{<i_{iph}>}{1 + Dm(k-1)} \quad (10)$$

$$<i_L> = \frac{<i_o>}{n(1-Dm)} \quad (11)$$

Maximum and minimum inductor current, (12) and (13), could be determined by the analysis of voltage across the inductor during the ON-state.

Table 1 – FC converter main converter requirements.

Output voltage (Vo)	100 V
Output power (Po)	500 W
Fuel cell (input) voltage (Vin)	24 V–42 V
Inductance and DC resistance (L-R)	30μH-10 mΩ
Diode forward voltage (Vd)	1 V
MOSFET on-resistance	50 mΩ
Output capacitor (Co)	590 μF
Switching frequency	100 kHz

$$i_{Lmax} = <i_L> + \frac{\Delta i_L}{2} = \frac{<i_o>}{n(1-Dm)} + \frac{V_{in}D}{2fL} \quad (12)$$

$$i_{Lmin} = <i_L> - \frac{\Delta i_L}{2} = \frac{<i_o>}{n(1-Dm)} - \frac{V_{in}D}{2fL} \quad (13)$$

Due to triangular and trapezoidal shapes of the branch currents, the input phase current ripple becomes large and dependent on k. During the ON-state, i_{iph} equals to k times i_L, while remains only i_L during the OFF-state, resulting in a current ripple given by (14).

$$\Delta i_{iph} = (k-1)\frac{<i_o>}{n(1-Dm)} + (k+1)\frac{V_{in}D}{2fL} \quad (14)$$

The current stresses of the different power semiconductors are easily derived from inductor and input phase currents. The maximum current for the MOSFETs, output diode, parallel-connection diodes and series-connection diodes are given by (15) and (16).

$$i_{Mmax} = k\left[\frac{<i_o>}{n(1-Dm)} + \frac{V_{in}D}{2fL}\right] \quad (15)$$

$$i_{Dmax} = i_{Dpmax} = i_{Dsmax} = \frac{< i_o >}{n(1-Dm)} + \frac{V_{in}D}{2fL} \quad (16)$$

The interleaving parallel connection of different phases (or modules) offers an effective method to provide power sharing, redundancy, improved dynamic response, but also input current ripple minimization, which is very desirable in fuel cell DC-DC power converters [16].

Because of the trapezoidal nature of the input phase currents, the effect of interleaving several currents results on an input current with the same average value but with smaller current ripple, as defined in (17) and (18). On the other hand, input current frequency is $n{\cdot}m$ times the switching frequency (19).

$$\Delta i_{in} = (k-1)\frac{< i_o >}{n(1-Dm)} + (k+1)\frac{V_{in}d}{2fL} \quad (17)$$

$$< i_{in} > = \frac{1+(k-1)Dm}{1-Dm} < i_o > \quad (18)$$

$$f_{i_{in}} = nmf \quad (19)$$

An exception of this rule happens in the cancellation points, which correspond to the duty cycles, D_{cc}, defined by (20). In those points, input current ripple exhibits triangular shape with minimum ripple, however, practical current ripple cancellation is very difficult to achieve because of the non-ideal behaviour of the different devices that defines the power converter.

$$D_{cc} = \frac{i}{n}; i = 1 \ldots (n-1) \quad (20)$$

The output current waveform is the same as the multi-device, interleaved boost [13], having the same input ripple current RMS value, given by (21), which is important to properly size the output capacitor, Co.

$$\Delta_{iout_{RMS}} = < i_{in} > \sqrt{[(Y - X/n)((X+1)/n - Y)] + n\Big/(12Y^2)((V_{in}t_{on})/(< i_{in} > L))^2\left[(X+1)^2(Y-X/n)^3 + X^2((X+1)/n - Y)^3\right]} \quad (21)$$

Where Y and X are given by (22) and (23), respectively

$$Y = m(T - t_{on})f \quad (22)$$

$$X = \lfloor nY \rfloor \quad (23)$$

Fuel cell converter evaluation: 4-IBC, 2-2 MIBC and 2-2-2 MISIBC

In this section, three different converter configurations have been evaluated for the Nexa Ballard PEM fuel cell requirements. In all cases, inductance value, switching

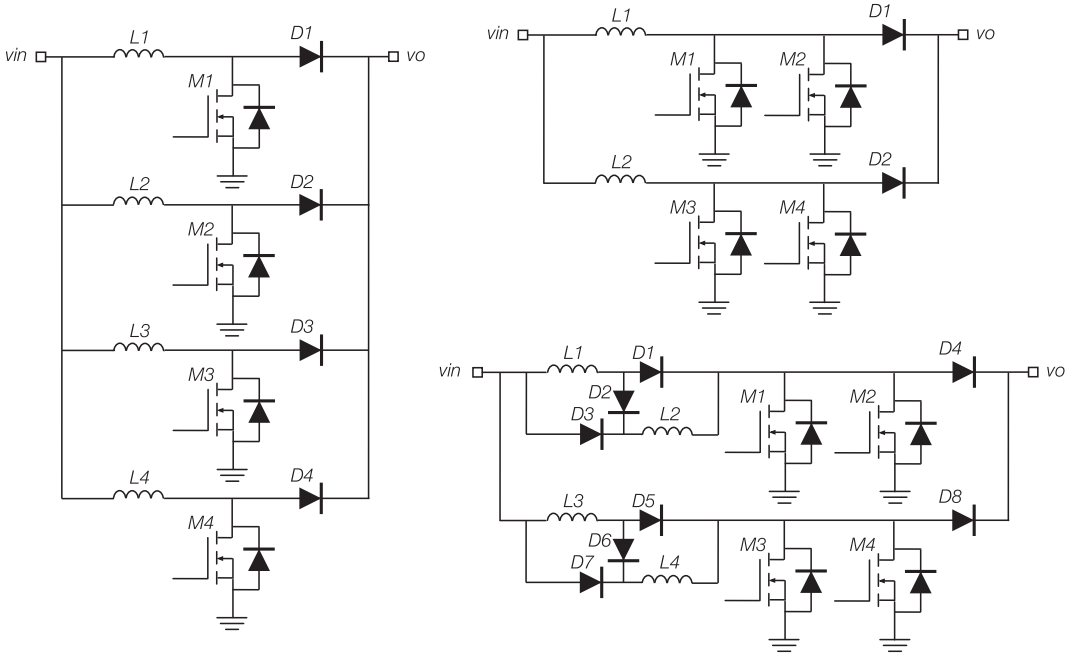

Fig. 5 – Three different converter configurations under evaluation: 4-IBC (left side); 2-2 MIBC (upper right); 2-2-2 MISIBC (lower right).

frequency, output power and DC voltage gain are kept the same, as listed in Table 1. Output voltage value is in accordance with current aerospace and microgrids applications. From Fig. 5, 4-IBC configuration refers to a 4-phase Interleaved Boost Converter [17]; 2-2 MIBC states for a 2-phase, 2-switch per phase Multi-Interleaved Boost Converter [13]; 2-2-2 MISIBC is a 2-phase, 2-switch per phase and 2 inductor switched-inductor network Multi-Interleaved, Switched-Inductor, Boost Converter.

Using PSIM electronic simulation software, the three selected converter configurations have been evaluated under similar working conditions, and the main results have gathered in Table 2.

As it can be observed from Table 2, the duty cycle of the 2-2 MIBC and 2-2-2 MISIBC is reduced 50% and 59% respectively compared to the 4-IBC. This fact is especially important to obtain high step-up voltage gain in non-isolated boost converters. On the other hand, the large number of diodes, which are operating under high-current conditions, strongly penalise the converter efficiency. Regarding the power semiconductor stress issues, it can be seen that structures with 2 phases exhibit larger RMS currents for the MOSFETs and output diodes, which is an indicator of the on-losses and a limiting factor for part selection. Obviously, the diodes of the switched-inductor network must be selected according to the maximum voltage and current carrying capabilities.

As it can be observed from Fig. 6, highly pulsated currents are found in the 2-2-2 MISIBC converter, due to the fact of different inductor charging and discharging paths, which establish trapezoidal current waveforms at phase level that cannot be cancelled with interleaving driving patterns. This forces to restrictive input filter design requirements for this topology.

Another important consideration for converter evaluation regards to part count, 2-2 MIBC offers an important advantage in terms of number of inductors, output diodes, current sensors and current error amplifiers if compared with the 4-IBC.

Table 2 – FC converter evaluation: main simulation results.

	4-IBC	2-2 MIBC	2-2-2 MISIBC
D	0.78	0.39	0.32
Efficiency	0.98	0.97	0.93
Δiin pk-pk	0.76 A	2.12 A	6.84 A
⟨<iL⟩>>	4.67 A	9.45 A	5.96 A
ΔiL pk-pk	6.07 A	3.00 A	2.38 A
iL frequency	100 kHz	200 kHz	200 kHz
Max. total L energy	3.54 mJ	3.58 mJ	3.02 mJ
iL rms	5.00 A	9.49 A	6.00 A
iM rms	4.40 A	5.85 A	6.80 A
iCo rms	2.13 A	4.77 A	2.73 A
iDo rms	2.37 A	4.64 A	3.58 A
iDp rms	N/A	N/A	4.81 A
iDs rms	N/A	N/A	3.58 A
vDp pk	N/A	N/A	40.12 V
vDs pk	N/A	N/A	21.52 V

Table 3 – 2-2-2 MISIBC 500-W FC prototype specifications and components.

Output voltage (Vo)	100 V
Output power (Po)	500 W
Fuel cell (input) voltage (Vin)	24 V–42 V
Inductance and DC resistance (L-R)	33uH-2.4 mΩ (WÜRTH WE 7443643300)
Power diodes	UJ2D1210T
MOSFET	SCT30KLGC11
Output capacitor (Co)	590 μF (CORNELL DUBILIER – 947D591K132DJRSN)
Input capacitor (Cin)	200 μF (2 × AVX FFV3 100 μF)
Switching frequency	100 kHz
PWM signals	Isolated drivers – Cypress PSoC 4 CY8CKIT-042

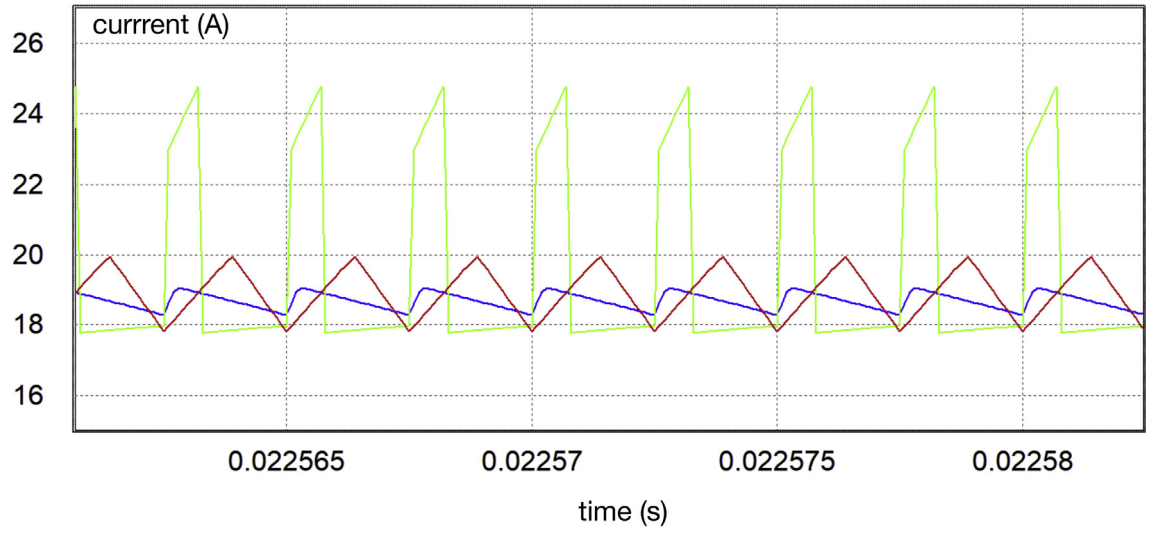

Fig. 6 – Input (fuel cell) current. Green trace: 2-2-2 MISIBC; red trace: 2-2 MIBC; blue trace: 4-IBC. (For interpretation of the references to color in this figure legend, the reader is referred to the Web version of this article.)

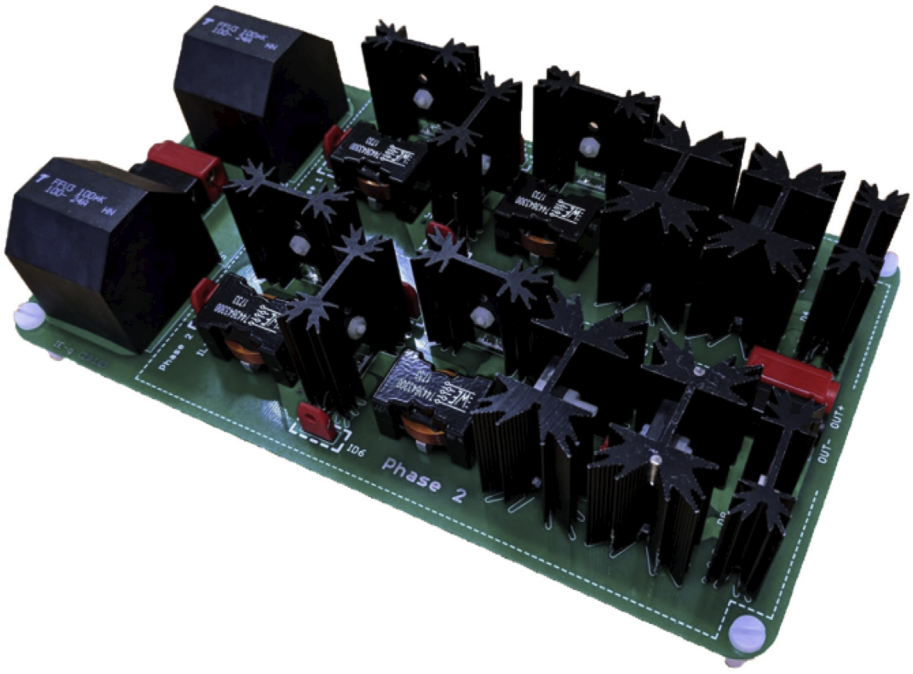

Fig. 7 – 2-2-2 MISIBC 500-W prototype.

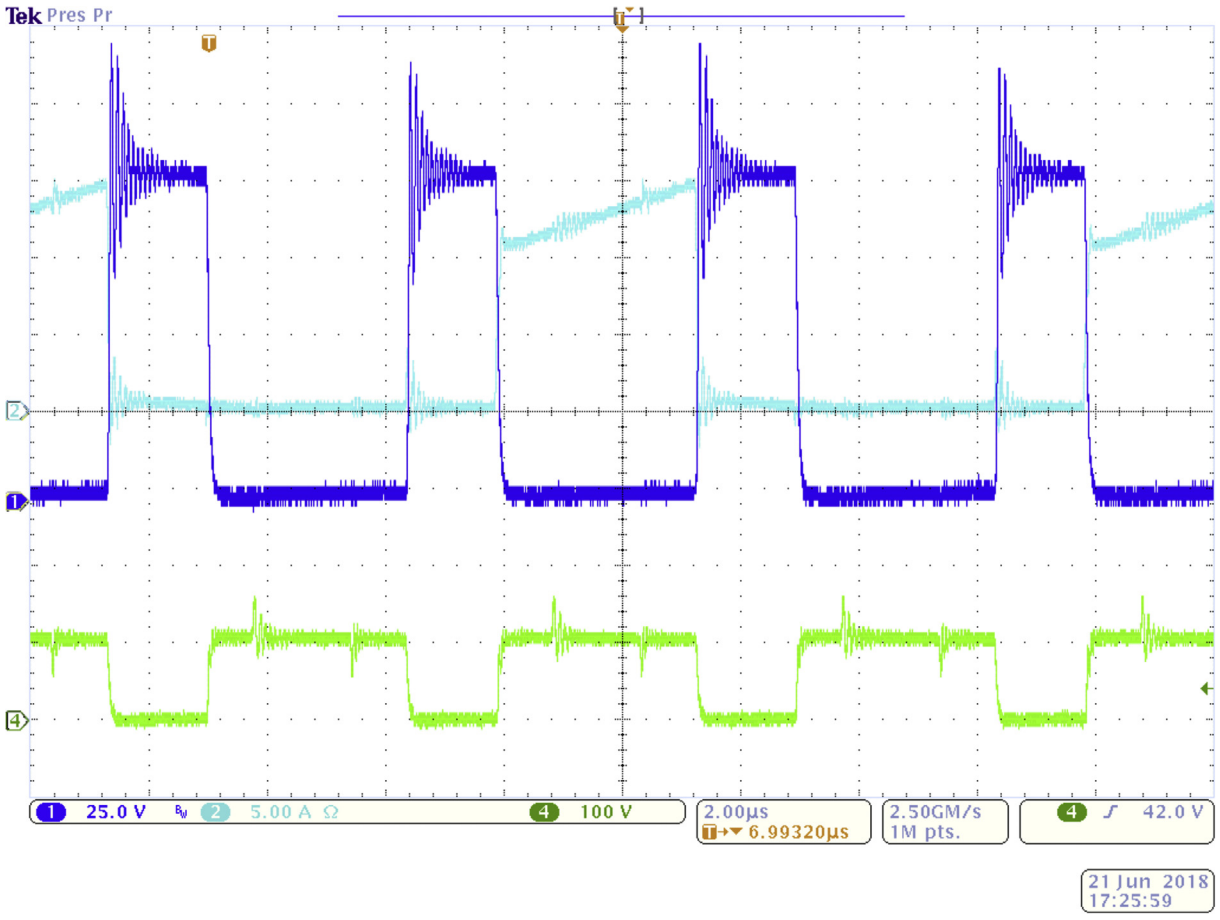

Fig. 8 – 2-2-2 MISIBC 500-W prototype, steady-state experimental waveforms, output boost section. Ch1: ph1-drain to source voltage. Ch2: ph1- MOSFET drain current. Ch4: ph1-output diode voltage.

The 2-2-2 MISIBC also keeps the same advantages for the output diodes, current sensors and current error amplifiers but it penalises in terms of total number of diodes required for the switched-inductor network.

Fuel cell converter experimental validation: 2-2-2 MISIBC

To verify the theoretical analysis and simulation results of the proposed MISIBC converter, a 2-2-2 MISIBC 500-W prototype has been built in the laboratory for use in a Nexa Ballard 1.2 kW fuel cell. The prototype specifications and components are collected in Table 3 and the photograph of the implemented circuit is shown in Fig. 7.

Some experimental measurements have been collected under the following operating conditions Vin = 24 V, D = 0.34, Vo = 102 V and Ro = 25 Ω. Fig. 8 illustrates the measured steady-state waveforms of the MOSFET and the output diode voltage of a single phase. It is observed that the drain to source voltage and diode voltage are switching twice faster than the MOSFET current, which indicates that the two MOSFETs are conducting alternately.

Fig. 9 includes the main steady-state waveforms of the switched-inductor network power semiconductors. It is shown that current raises during the MOSFET on-time through the parallel diodes and decreases during the off-time through the series diode. The series diode blocks Vin and the parallel diode (Vo-Vin)/2, as predicted.

Fig. 10 shows the input current waveforms. It is clearly appreciated that phases currents have trapezoidal shapes with phase displacement because of the interleaving driving. The resultant input current has a current ripple equal to single phase but twice DC value, indicating that input current ripple does not increase with the number of paralleled phases. On the other hand, the input current frequency is 400 kHz that results from applying (19) with 100 kHz switching frequency.

To conclude this section, some efficiency and DC measurements have been reported in Table 4. Higher efficiencies are obtained at lower output power, due to lower current circulating through power diodes. Output voltage is also affected because of forward diode voltage variations with current.

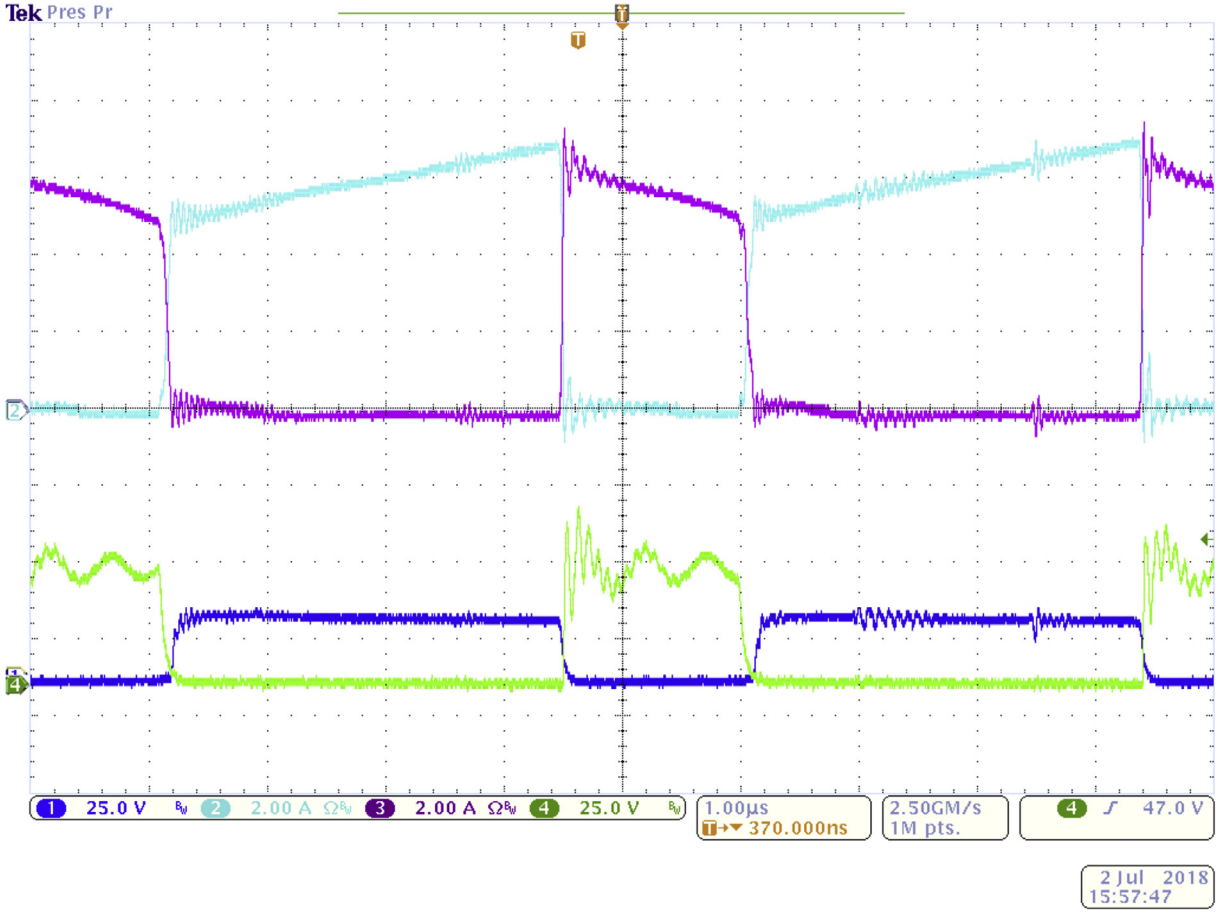

Fig. 9 – 2-2-2 MISIBC 500-W prototype, steady-state experimental waveforms, switched-inductor network. Ch1: ph1-series diode voltage. Ch2: ph1-parallel diode current. Ch3: ph1 – series diode current. Ch4: ph1-parallel diode voltage.

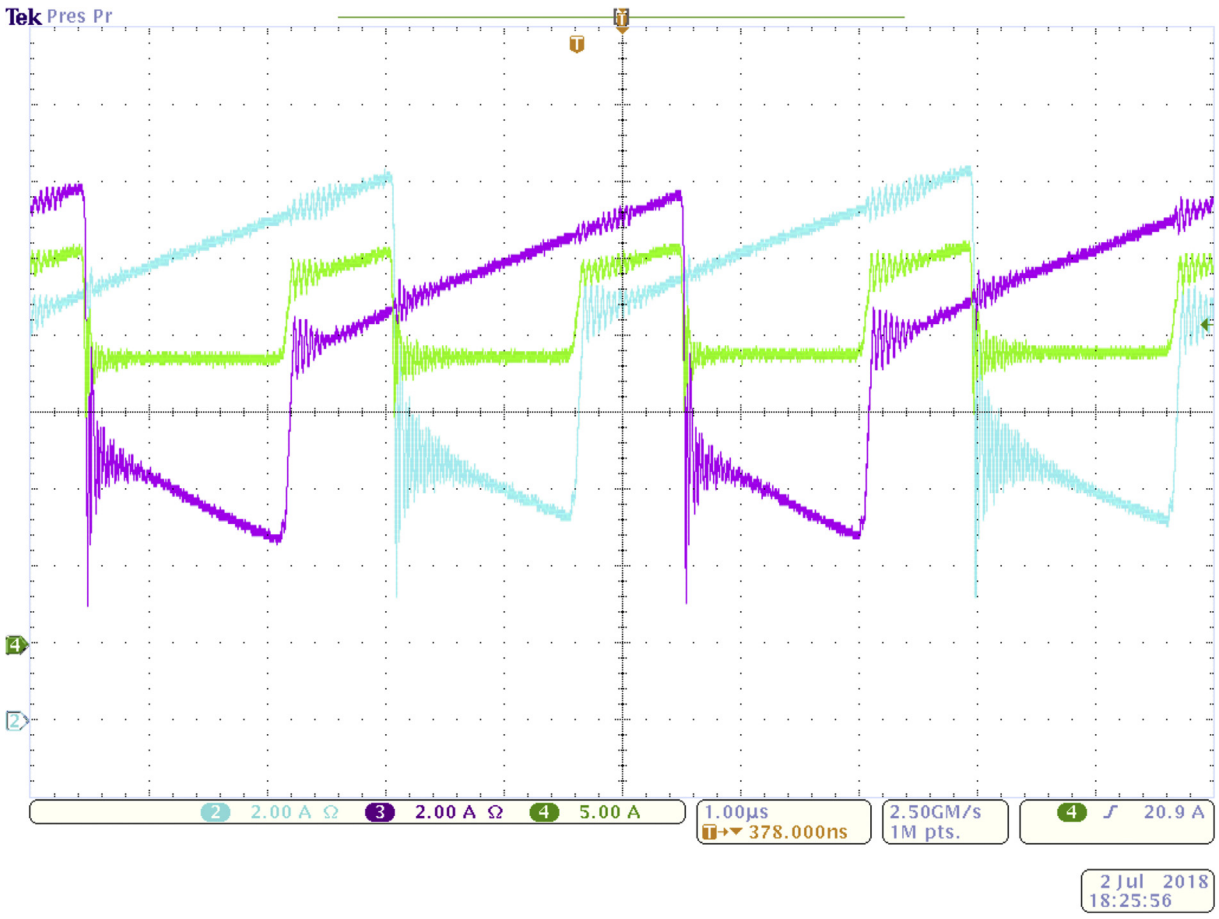

Fig. 10 – 2-2-2 MISIBC 500-W prototype, steady-state experimental waveforms, input currents. Ch2: ph1-input current. Ch3: ph2 – input current. Ch4: input current.

Table 4 – 2-2-2 MISIBC 500-W experimental results: DC measurements.

Load	<Vin>	<Iin>	<Vo>	<Io>	Efficiency
100 Ω	24 V	5.95 A	115.5 V	1.16 A	0.94
55 Ω	24 V	11.61 A	110.8 V	2.17 A	0.86
33 Ω	24 V	15.90 A	105.7 V	3.12 A	0.86
25 Ω	24 V	20.50 A	101.5 V	3.99 A	0.82

Conclusions

This paper presents an alternative to IBC and MIBC converters when high step-up voltage ratio is required, which in fact is very common in fuel cell LVDC distribution applications. The presented converter has the following attractive characteristics:

- Current sharing issues at phase level are overcome by forcing the conduction of only one power semiconductor at a given time and reducing its duty cycle. Then, thermal management at phase level could be simplified.
- Different switching, inductor and input/output currents are obtained, which makes possible a converter optimization depending on different parameters and specifications.
- Switched-inductor networks allow high step-up voltage ratio with repeatable structures. The order of the network could be selected depending on the converter requirements.

In summary, a high versatile boost converter has been presented with three adjusting parameters, m – number of power transistors per phase; n – number of phases and k-order of the switched-inductor network. This structure is specially adapted for medium power fuel cell power conditioners.

Derivation of MISIBC steady-state equations, evaluation and simulation of three different interleaved boost structures, 4-IBC, 2-2 MIBC and 2-2-2MISIBC has been carried out for Nexa Ballard 1.2 kW fuel cell specifications. Finally, a 500-W 2-2-2 MISIBC prototype has been implemented and tested at Vin = 24 V and Vo = 100 V. Experimental results show that MISIBC is an interesting alternative for non-isolated, high step-up voltage ratio DC-DC conversion.

To conclude, further studies will be orientated to overcome the negative effect of diode losses on the switched-inductor networks as well as to provide soft-switching methods to power semiconductors. This will allow the increase of the voltage conversion ratio for higher DC busses, e.g. 400 Vdc, with high power conversion efficiency.

REFERENCES

[1] Elsayed AT, Mohamed AA, Mohammed OA. DC microgrids and distribution systems : an overview. Elec Power Syst Res 2015;119:407–17. https://doi.org/https://doi.org/10.1016/j.epsr.2014.10.017.

[2] Rodriguez-DIaz E, Savaghebi M, Vasquez JC, Guerrero JM. An overview of low voltage DC distribution systems for residential applications. In: Proceedings of the 5th IEEE international conference on consumer electronics (IEEE ICCE-Berlin 2015) publication. IEEE; 2015. p. 318–22. https://doi.org/10.1109/ICCE-Berlin.2015.7391268.

[3] Cetin E, Yilanci A, Ozturk HK, Kasikci I, Colak M, Icli S. Construction of a fuel cell system with DC power distribution for residential applications. Int J Hydrogen Energy 2011;36(17):11474–9. https://doi.org/10.1016/j.ijhydene.2010.11.072.

[4] Rosas-Caro JC, Sanchez VM, Valdez-Resendiz JE, Mayo-Maldonado JC, Beltran-Carbajal F, Valderrabano-Gonzalez A. Quadratic buck-boost converter with positive output voltage and continuous input current for PEMFC systems. Int J Hydrogen Energy 2017;42(48):30400–6. https://doi.org/https://doi.org/10.1016/j.ijhydene.2017.10.079.

[5] Guilbert D, Gaillard A, Mohammadi A, N'Diaye A, Djerdir A. Investigation of the interactions between proton exchange membrane fuel cell and interleaved DC/DC boost converter in case of power switch faults. Int J Hydrogen Energy 2015;40:519–37. https://doi.org/10.1016/j.ijhydene.2014.10.072.

[6] Blaabjerg F, Chen Z, Kjaer SB. Power electronics as efficient interface in dispersed power generation systems in dispersed power generation systems. IEEE Trans Power Electron 2004;19(5):1184–94. https://doi.org/10.1109/TPEL.2004.833453.

[7] Guilbert D, N'Diaye A, Gaillard A, Djerdir A. Fuel cell systems reliability and availability enhancement by developing a fast and efficient power switch open-circuit fault detection algorithm in interleaved DC/DC boost converter topologies. Int J Hydrogen Energy 2016;41(34):15505–17. https://doi.org/10.1016/j.ijhydene.2016.01.169.

[8] Giral R, Martínez-Salamero L, Singer S. Interleaved converters operation based on CMC. IEEE Trans Power Electron 1999;14(4):643–52. https://doi.org/10.1109/63.774201.

[9] Hegazy O, Van Mierlo J, Lataire P. Analysis , modeling , and implementation of a multidevice interleaved DC/DC converter for fuel cell hybrid electric vehicles. IEEE Trans Power Electron 2012;27(11):4445–58. https://doi.org/10.1109/TPEL.2012.2183148.

[10] Axelrod B, Berkovich Y, Ioinovici A. Switched-capacitor/switched-inductor structures for getting transformerless hybrid DC – DC PWM converters. IEEE TCS-I: Regular Papers 2008;55(2):687–96. https://doi.org/10.1109/TCSI.2008.916403.

[11] Yang L, Liang T, Chen J. Transformerless DC – DC converters with high step-up voltage gain. IEEE Trans Ind Electron 2009;56(8):3144–52. http://doi.org/10.1109/TIE.2009.2022512.

[12] Renken F, Pop-Calimanu I-M, Schürmann U. Novel multiphase hybrid boost converter with wide conversion ratio keywords multiphase hybrid boost DC/DC converter. In: European conference on power electronics and applications. IEEE; 2014. p. 1–10. https://doi.org/10.1109/EPE.2014.6910967.

[13] Garrigós A, Sobrino-Manzanares F. Interleaved multi-phase and multi-switch boost converter for fuel cell applications. Int J Hydrogen Energy 2015;40(26):8419–32. https://doi.org/10.1016/j.ijhydene.2015.04.132.

[14] Sobrino-Manzanares F, Garrigós A. An interleaved, FPGA-controlled, multi-phase and multi-switch synchronous boost converter for fuel cell applications. Int J Hydrogen Energy 2015;40(36):12447–56. https://doi.org/10.1016/j.ijhydene.2015.07.078.

[15] Erickson RW, Maksimovic D. Fundamentals of power electronics. 2nd ed. Springer US; 2001. http://doi.org/10.1007/b100747.

[16] Fardoun AA, Hejase HAN, Al-Marzouqi A, Nabag M. Electric circuit modeling of fuel cell system including compressor effect and current ripples. Int J Hydrogen Energy 2017;42(2):1558–64. https://doi.org/10.1016/j.ijhydene.2016.07.093.

[17] Garrigós A, Blanes JM, Lizán JL. Non-isolated multiphase boost converter for a fuel cell with battery backup power system. Int J Hydrogen Energy 2011;36(10):6259–68. https://doi.org/10.1016/j.ijhydene.2011.01.153.